An Explanation for Neptune's Ring Arcs

CAROLYN C. PORCO

The Voyager mission revealed a complex system of rings and ring arcs around Neptune and uncovered six new satellites, four of which occupy orbits well inside the ring region. Analysis of Voyager data shows that a radial distortion with an amplitude of approximately 30 kilometers is traveling through the ring arcs, a perturbation attributable to the nearby satellite Galatea. Moreover, the arcs appear to be azimuthally confined by a resonant interaction with the same satellite, yielding a maximum spread in ring particle semimajor axes of 0.6 kilometer and a spread in forced eccentricities large enough to explain the arcs' 15-kilometer radial widths. Additional ring arcs discovered in the course of this study give further support to this model.

STELLAR OCCULTATIONS OBSERVED FROM THE EARTH IN THE mid-1980s indicated the existence of incomplete narrow rings, or ring arcs, around the planet Neptune (*1*). In the belief that these features might be long-lived and stable, a confinement mechanism was proposed that anchored the arcs at particular radial and longitudinal locations defined by orbital resonances of a single nearby shepherding satellite (*2*). Preliminary examination of imaging data obtained during the Voyager/Neptune encounter in August 1989 showed Neptune's outermost narrow ring, 1989N1R, to contain three arc features clustered within 33° of orbital longitude, with normal optical depths $\tau_N \sim 0.1$, azimuthal extents of approximately 4°, 4°, and 10°, for leading, middle, and trailing arcs, respectively, and separations (center-to-center) of approximately 13° (*3*). A fortuitous stellar occultation by the arcs observed by the Voyager ultraviolet spectrometer (UVS) and photopolarimeter (PPS) experiments yielded a $\tau_N \sim 0.05$ and confirmed the ~15-km arc radial widths observed from the ground (*4*). It was determined that the Voyager-observed arc cluster was responsible for most of the successful ground-based occultation events (*3, 5, 6*), indicating an arc lifetime longer than the time required for 15 km–wide ring material to spread by means of differential mean motion over 360° and form a complete ring. Voyager images captured six new Neptunian satellites, four of which fall well within the ring region. However, initial searches for a dynamical relation between the arcs and the nearest inner satellite, Galatea (1989N4), based on preliminary satellite orbital elements led to the conclusion that the single-satellite arc confinement mechanism was not at work in this ring system, leaving the existence of Neptune's apparently stable arcs a mystery (*7*).

Using the ephemeris describing Voyager's passage through the Neptune system and the resulting Neptune orientation and gravitational parameters (*8*), none of which was available in final form until 9 months after the Voyager encounter, Owen *et al.* (*9*) analyzed sequences of Voyager images of the six new satellites to obtain precise orbital elements. Satellite sizes have also been measured in these images (*10*) allowing estimates of satellite masses. This new information, together with the realization that the arcs may not be occupying consecutive corotation sites (rendering irrelevant the mismatch between the observed 13° arc separation and that expected from corotational shepherding by Galatea) has motivated a careful analysis of Voyager arc images and a reexamination of the dynamical relations between the arcs and satellite. It is shown here that the single satellite arc shepherding model, with Galatea playing the starring role, may be the most plausible explanation for the confinement of Neptune's ring arcs.

Lindblad and corotation resonances near 1989N1R. The single satellite model requires the azimuthal and radial confining action of the corotation and Lindblad resonances, respectively, of a nearby satellite on a set of ring particles. All corotation resonances occur at radial locations where the mean orbital motion, n, of the perturbed particle equals the pattern speed, Ω_p^c, of the perturbing potential. Such resonances lead to slow libration around a mean orbit guiding center, or corotation site, by exciting periodic variations in semimajor axis, a, and in longitude, λ. In the frame rotating with the pattern speed, the particle's libration takes the form of an ellipse, the minor axis of which may be identified with the corotation resonance width, W_c. The strongest corotation resonances produced by a satellite are associated only with the satellite's angular motion, n_s: that is, $\Omega_p^c = n_s$. Familiar examples of these are the triangular Lagrange points, L_4 and L_5, which lead and trail the satellite in its orbit by 60°. The next strongest corotation resonances are those associated with either satellite eccentricity only (CER) or satellite inclination only (CIR). For example, CIR resonances located at radial distances greater than that of the satellite's orbit, the Galatea-arc geometry observed at Neptune, have pattern speeds obeying the relation $m_c\Omega_p^c = (m_c - 1)n_s + \dot{\Omega}_s$, where $\dot{\Omega}_s$ is the satellite nodal precession rate and the positive integer, m_c, is the corotation resonance wave number.

For $m_c \gg 1$, each corotation resonance is situated very near a Lindblad resonance of the same satellite. These resonances excite variations in the particle's longitude of periapse, ϖ, and eccentricity, e. The strongest Lindblad resonances always have pattern speeds equal to the mean motion of the satellite, $\Omega_p^L = n_s$, and for an interior satellite are located where $m_L\Omega_p^L = (m_L + 1)n - \dot{\varpi}$. Here, $\dot{\varpi}$ is the particle's apsidal precession rate. The width of such resonances is given by $W_L \sim (M_s/M_p)^{1/2} a_s$, where M_s and M_p are the masses of satellite and planet, respectively, and a_s is the satellite orbital semimajor axis (*11*). The Lindblad resonance wave number, m_L, differs from the wave number, m_c, of the nearest corotation resonance by ± 1.

The $2m_c$ stable equilibria distributed around the orbit of a

The author is in the Department of Planetary Sciences, University of Arizona, Tucson, AZ 85721.

Table 1. Low-order resonances of Galatea near the N1R ring based on the satellite's orbital elements (*9*). The widths were calculated by using a mutual inclination $i_m = 0.03°$ and a libration ellipse major axis of 4° for the CIR only, and a satellite mass determined from this work for both CIR and OLR.

Type	Wave number (m_L or m_c)	Radius (km)	Width (km)
42:43 CIR	43	62932.48 ± 0.13	0.6
42:43 OLR	42	62930.83 ± 0.13	9

corotation resonance are sites of potential maxima where interparticle collisions, and the attendant loss of energy, would cause any ring material that had collected there to spread both in radius and azimuth. The nearby Lindblad resonance delivers the orbital energy required to maintain ring particle libration around the corotation site by exerting repulsive torques on the ring material: those particles on the satellite side of their libration ellipses undergo a larger repulsion than do those on the anti-satellite side. The resulting differential torque across the corotation site serves to stabilize the material there and form a stable ring arc. The Lindblad resonance perturbs the libration of particles around the corotation site by causing the orbit of the libration center to become elliptical.

The aforementioned conditions for resonance and expressions for pattern speed may be used to locate the resonances of a satellite. The resonance types, wave numbers, radial locations, uncertainties (due primarily to uncertainties in satellite mean motion), and radial widths of Galatea's strongest CIR and OLR falling closest to 1989N1R are given in Table 1. The separation of resonances of the same type but with wave numbers differing by 1 is $3(a - a_s)^2/2a_s$ = 23 km (*11*), greater than the width of either the corotation or Lindblad resonance and greater than the arcs' width. The resonances of each type are isolated. Using the latest Neptune gravity coefficients (*8*), one obtains a semimajor axis inferred from the arcs' mean motion [820.1185 ± 0.0004° per day (*5*)] of a = 62932.37 ± 0.02 km. The location of the 42:43 CIR with m_c = 43 is coincident with this value, considering the stated uncertainties and the CIR resonance width; the 42:43 OLR with m_L = 42 falls 1.5 km interior to the ring's centerline. These results alone suggest the existence of the proper environment for single-satellite arc shepherding of Neptune's arcs. In what follows, results obtained from Voyager data analysis are compared with theoretical predictions of the behavior of ring particles shepherded in this manner to elucidate the plausibility of this model (*12*).

Radial excursions versus longitude. Voyager's highest resolution images of the Neptune rings were part of a series that was retargeted to the arcs after previous Voyager imaging observations had been used to determine the arcs' positions and approximate mean motion (*3*). Eighteen clear filter frames comprising five sets taken at distinctly different times (and therefore imaging resolution) were recorded during the time interval from −12 hours to +18 hours from Neptune closest approach.

In order to examine the shapes and kinematics of the arcs in detail, absolute radii and longitudes were obtained from the Voyager UVS stellar occultation datum and across all 18 high-resolution images after errors in camera pointing were corrected by stellar navigation. The longitude system used for these measurements is Neptune centered with its origin taken to be the ascending node of the Neptune equator on the Earth Mean Equator of 1950 (EME50) at the time of Voyager Neptune encounter. [This system is referred to below as the Jacobson system (*8*).] In general, imaging measurements were made at 1° intervals in radial scans averaged over 0.5° in longitude, yielding typically 7 individual measurements on a narrow angle (NA) frame and 17 measurements on the highest resolution wide-angle (WA) frame used in this analysis (*13*). Almost all images of the arcs were smeared both in the radial and longitudinal directions because of camera motion during the exposure, making the determination of the scan's center radius difficult by visual inspection. Consequently, each scan was modeled by a Gaussian function, a very good approximation in most cases to the scan's profile, to yield a center radius taken to be the mean of the Gaussian and a (relative) radial uncertainty taken to be several standard errors in the Gaussian mean. The latter was always much less than the width of the Gaussian and therefore much less than the radial smear. (The absolute radial uncertainty for each image included the error associated with uncertainty in the stellar navigation process.)

Motivated by the expectation that Galatea would be perturbing the arcs through its 42:43 OLR, a model describing an m_L = 42 pattern precessing through the ring at the expected pattern speed was used to fit 66 reliable radius-longitude measurements on the arcs. [The model incorporated the effects of inclination to account for the possibility that N1R might be inclined to the Neptune equator determined from Voyager trajectory analyses (*8*).] The resulting four free parameters of the model, which describes the configuration of the ring at the chosen epoch, are: radial amplitude, ae = 29.6 ± 1.5 km; eccentricity, e = 0.00047 ± 0.00002; longitude of radial minimum, ϖ_0 = 50.82° ± 0.10°; inclination, i_0 = 0.0617° ± 0.0043°; longitude of the node, Ω_0 = 102.2° ± 1.0° (*14*). A model including an m = 1 normal mode (*15*) instead of inclination gave significantly poorer residuals. The deviations of mean radius observed in all images from a constant value are undoubtedly due to an inclination.

The model was fitted to three images of the trailing arc at −7.2 hours from closest approach from a spacecraft-planet range of ~4.8 × 10^5 km (Fig. 1). The ring radial scale is ~7.5 km/pixel. The longitudes of the data points have been precessed back to epoch by using the solution pattern speed: that is, Galatea's mean motion. The error associated with this precession is <0.02°. Radial excursion is given relative to the mean projected radius for that set of frames. A 29.6-km radial distortion with azimuthal wavelength of $360/m_L$ = 8.57143° is clearly seen. All high-resolution images of the arcs show this traveling distortion. (At present, there is no definitive evidence that this distortion is seen traveling through any part of the outer

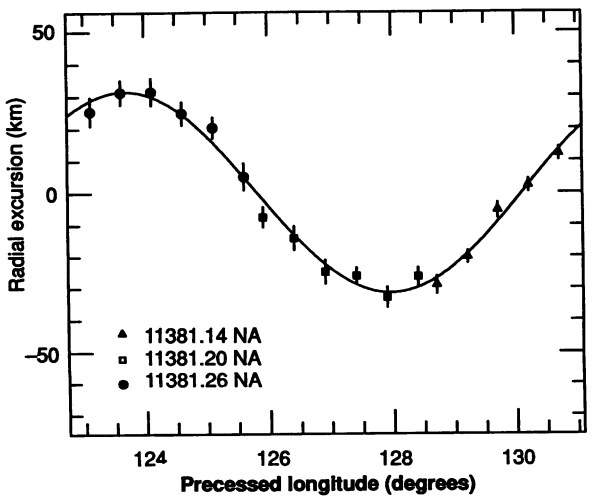

Fig. 1. The measurements of longitude and radial excursion made on the trailing arc as imaged in three narrow angle Voyager frames taken 7.2 hours before Voyager closest approach to Neptune. All data points have been precessed back to a common epoch by using a pattern speed Ω_p^L = 839.6598° per day (*9*). The solid line indicates a portion of the m_L = 42 pattern which best fits the data.

ring other than that containing the arcs.) Figure 2 shows the orientation of the pattern together with the position of the satellite at epoch. All Voyager high-resolution imaging data, reduced to show this distortion and precessed under the pattern speed to the epoch, are also shown. (These positions are not to be confused with the positions of the arcs at this time. They merely show the indicated portion of the traveling radial distortion that was imaged passing through the arcs when Voyager imaging observations were made.)

The longitude of Galatea at epoch in the Jacobson reference system is calculated to be $\lambda_s = 46.64° \pm 0.01°$. [Galatea's orbital elements are given relative to the satellite's Laplace plane (*9*). Hence a coordinate transformation from the Laplace system to the Jacobson system is necessary to compare Galatea's elements with all longitudes measured and determined in this article. One of the 42 radial minima of the pattern at epoch falls at $\varpi_0 = 50.82° \pm 0.1°$. For ring orbits exterior to Galatea's 42:43 OLR, the Lindblad resonance critical argument $\Psi_L = \pi$. Therefore, the longitude at epoch of conjunction between satellite and ring particles occurs at $\lambda = \varpi_0 + \Psi_L/m_L = 46.53° \pm 0.10°$, identical within uncertainties to λ_s. The $m_L = 42$ pattern and satellite have the relation anticipated for radial perturbation by Galatea's 42:43 OLR if all of the particle orbits are exterior to this resonance. (The fact that the difference between the arc's semimajor axis and the OLR, ~1.5 km, is much less than the arcs' width is discussed below.)

One may use the observed eccentricity and Eqs. 16 and 17 of Goldreich *et al.* (*2*) to determine the satellite's mass: $M_s = (2.12 \pm 0.08) \times 10^{21}$ g. Utilizing measurements of Galatea's size obtained from Voyager image analysis [$r = 79 \pm 12$ km (*10*)], one obtains a density, $\rho_s = 1.0 \pm 0.5$ g cm^{-3}; the uncertainty arises predominantly from the 15% uncertainty in the satellite's radius. This result falls within the range of reasonable densities expected in the Neptune system (*16*).

Discovery of additional arcs. In the course of this analysis, additional arcs were discovered in the outer ring in Voyager high- and low-resolution images. A portion of a low-resolution WA frame shows the entire arc region seen in a forward-scattered geometry (Fig. 3). The smear in this 255.4-s exposure has a large component perpendicular to the longitudinal direction in the arc region, aiding the detection and measurement of reasonably bright and longitudinally variable features in the ring. Three stars shining through the ring can be distinguished from arcs by their differing smear direction.

A radially averaged azimuthal scan was taken through the arc region of FDS 11415.45 and precessed back to epoch under the arcs' mean motion (Fig. 4). Dark current and a steep gradient across

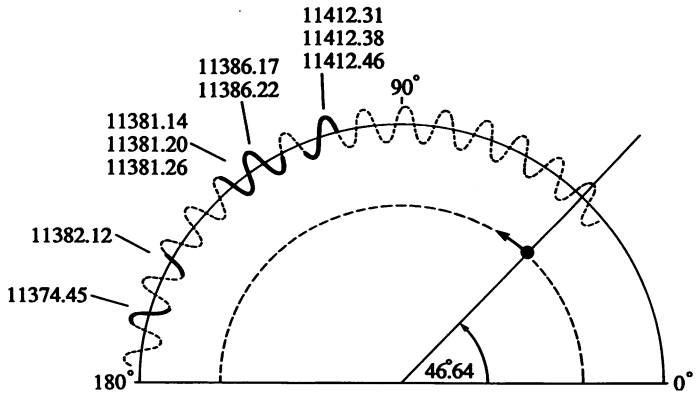

Fig. 2. The orientation of the $m_L = 42$ pattern and the position of Galatea on 18 August 1989, 12:00 ephemeris time. Voyager observations of this pattern as it was imaged passing through the arcs at the time of the high-resolution retargetted frames are shown as solid lines.

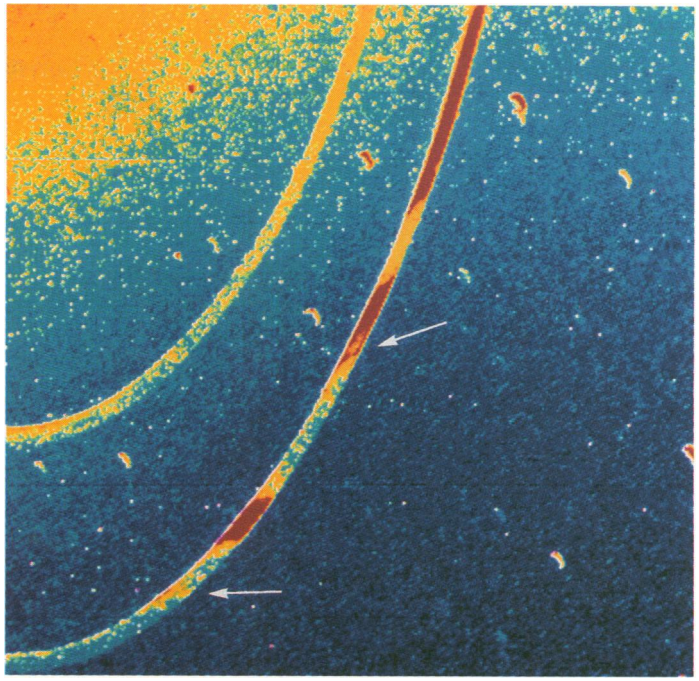

Fig. 3. An image-processed portion of a wide-angle 255.4-s Voyager image (FDS 11415.45), taken 20.5 hours after closest approach to Neptune from a range of 1.3 million kilometers and a phase angle of 135°, showing the arc region. In this colorized version, red is brighter than yellow. Orbital motion is clockwise. The newly discovered arcs are indicated by arrows. The leading arc, A1, is almost entirely yellow. The shoulder arc, A3, appears narrow and red and is separated from A4 by a yellow "depression." The "crescent moons" are stars smeared by spacecraft motion during the exposure.

this scan, attributable to the steep gradient in scattered light from Neptune in this frame, were removed to produce Fig. 4. Asterisks indicate the positions of stars; the symbol r, the position of an incompletely removed camera reseau. A new leading arc can be found at ~285°. The shape of the feature at ~264° is particularly asymmetrical, an observation that is reproducible in all images of this feature, and it appears to be two arcs side by side (Fig. 3). In total there are five arcs whose edges have been measured in this scan and from which longitude centers, full longitudinal lengths at half maximum brightness (FLHM), and center-to-center separations have been determined (Table 2). Their unofficial designations used in this article, from leading to trailing, are: A1, A2, A3, A4, and A5.

If the particle properties in all arcs are the same, the optical depths of the newly discovered arcs may be estimated by comparing their brightnesses to those of the arcs that were observed from the ground. Arc A4 was apparently observed in a stellar occultation on 22 July 1984 (*5*). For $W_r = 15$ km, the equivalent depth observed on this date ($W_r\tau_N \sim 2$ km) yields $\tau_N \sim 0.13$. This result implies an optical depth for A1, the new leading arc, of roughly $\tau_N \sim 0.04$, and roughly twice that, $\tau_N \sim 0.08$, for A3, the shoulder arc.

Azimuthal confinement by Galatea. The results presented in the previous sections indicate beyond doubt that Galatea is perturbing the arcs through its 42:43 OLR. In order for the single satellite model to provide a complete explanation of Neptune's ring arcs, it remains to be shown that the same satellite is azimuthally shepherding the set of arcs observed in Voyager data.

The variation of ring brightness with longitude along the arcs (Fig. 4) suggests the action of an $m_c = 43$ corotation-inclination resonance. If the arcs are falling within the corotation zones of Galatea's 42:43 CIR, then one might expect them to have angular extents $< 360/2m_c = 4.1860°$. The FLHM's (Table 2) of A1, A2, A3, and A4 all meet this criterion to varying degrees. Only the

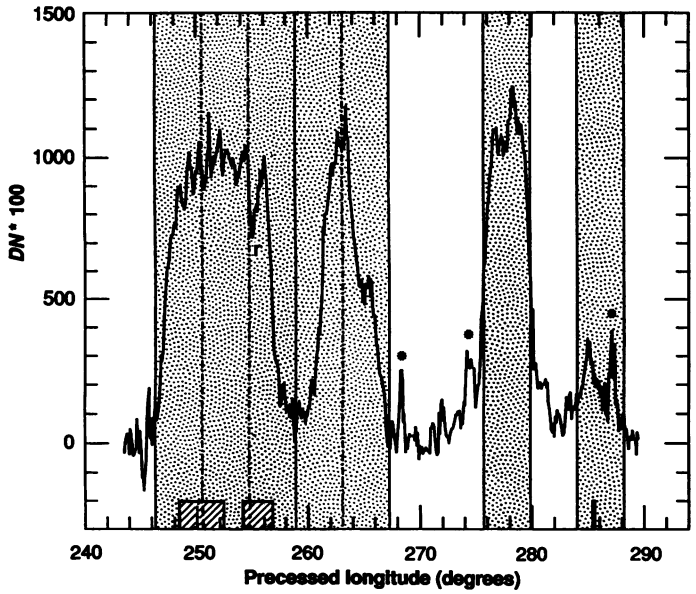

Fig. 4. A radially averaged longitudinal scan of the arc region as seen in image FDS 11415.45 (Fig. 3) and precessed back to epoch using the arcs' mean motion, n = 820.1185° per day (*5*). The asterisks indicate the positions of stars; the symbol **r** indicates an incompletely removed camera reseau.

angular extent of A5, 9.6°, is between twice and three times this value. Moreover, although the arc separations are not exact integer multiples of 4.186°, if the observed features are interpreted as a series of arcs confined by Galatea's CIR, they imply that A1 and A2 are 2 corotation sites apart, A2 and A3 are 3 corotation sites apart, and A3 and A4 are occupying adjacent sites. The trailing arc, A5, may be two or three adjacent corotation sites in angular extent. One possible array of properly spaced corotation zones falling on the arc region is indicated in Fig. 4 as a set of stippled regions. The observed structure within the ring roughly matches that expected for Galatea's m_c = 43 CIR provided that not all consecutive corotation sites are filled.

Why do the separations between the observed arcs not exactly match the expected scale of 4.186°? Preliminary photometric modeling of Neptune's rings suggests that they are extremely dusty relative to the rings of Saturn and Uranus and that the majority of dust in the arcs is more likely to come from collisions among bigger "source" bodies than from meteroid bombardment (*3*). The libration periods of these bodies can be calculated with Eqs. 3 and 7 of Goldreich *et al.* (*2*) and are approximately 10 years, much longer than an orbital period and probably much longer than the lifetime of any one dust particle. If the dust comprising the bulk of the observed material has its source in bigger bodies, then it is possible that for arcs in which these bodies are sparse and have an uneven longitudinal distribution, the 10-year circulation around a corotation site might alter the position of the observed arc within its corotation zone. This would be especially true for the smallest arcs: A1, A3, and A4 might be such examples. The longer, more optically thick arcs may be those for which there are a greater number of confined big particles. In this regard, the "best behaved" arc feature is considered to be A2: it is comparatively optically thick and longitudinally fills its corotation zone, perhaps indicating an even and substantial distribution of large bodies. Consequently, its appearance and position over a libration period would be observed to be stable. For these reasons, the best fitting phase of corotation sites due to Galatea is chosen so that A2 is centered in a corotation zone. (However, there is a great deal of ambiguity in the choice of phase and any value within a range of ~±1° of the one indicated might be considered equally plausible.)

In principle, one may compare this phase with the expected phase of Galatea's CIR. To accomplish this, the corotation potential in the Jacobson system at epoch must be examined. The potential reaches a maximum, the stable equilibrium configuration for corotation resonances, when cos $\Psi_c = -1$, and the CIR critical argument $\Psi_c = 2[m_c\lambda - (m_c - 1)\lambda_s - \Omega_s] = \pi + 2\pi l$. (Here, Ω_s is the nodal line of the satellite on the ring plane and l is an integer which ranges from 0 to $2m_c - 1$: that is, there are $2m_c$ = 86 corotation sites around the ring separated by $360/2m_c$ = 4.186°.) Taking m_c = 43, and knowing $\lambda_l(t_0)$, the longitude of the lth potential maximum at time t_0, we may solve for $\Omega_s(t_0) = 43\lambda_l(t_0) - 42\lambda_s(t_0) - \pi/2 - \pi l$. All even l's yield the same satellite node; odd l's yield a node differing by 180°. Utilizing the epoch longitude of A2, λ = 277.73° ± 0.05°, $\Omega_s(t_0)$ = 353.5° (173.5°) ±2.2° for an odd (even) corotation site. It is illuminating to compare this satellite nodal line with that determined from the modeling results given earlier. The inclination and nodal line of the ring plane in the Jacobson system found from this work, i_0 = 0.0617° ± 0.0043° and Ω_0 = 102.2° ± 1°, imply a ring pole in EME50 coordinates of $\alpha_{50}(r)$ = 298.9398° ± 0.006° and $\delta_{50}(r)$ = 42.8249° ± 0.002°. The orbit normal of Galatea is $\alpha_{50}(s)$ = 298.9226° ± 0.014° and $\delta_{50}(s)$ = 42.8127° ± 0.014° (*9*). The longitude system used in this work has as its EME50 pole $\alpha_{50}(J)$ = 298.8575° and $\delta_{50}(J)$ = 42.8118°. Thus, the mutual inclination of ring and satellite orbits is i_m = 0.02° ± 0.01°, and the ascending node of the satellite on the ring is Ω_s = 314° ± 45°. (The value of i_m is much larger than the angular difference in the calculated Laplace poles of Galatea and the arc ring.) The large nodal line uncertainty, a result of the small mutual inclination, makes it impossible to conclude unambiguously that A2 is centered on an odd corotation site despite the fact that the nominal observed satellite nodal line agrees within errors with that determined under this assumption. Consequently, while the azimuthal spacing of the arcs appears roughly correct, the exact phase of the pattern is uncertain.

However, there are other circumstantial indications that azimuthal shepherding is confining the arcs. Consider the significance of the small mutual inclination between Galatea and the ring, i_m = 0.02° ± 0.01°. Statistically, this value is consistent with zero, and in such a case there would be no corotational shepherding whatsoever. On the other hand, assuming an upper limit to the inclination of i_m = 0.03° and taking a typical arc length to be ~4°, the amplitude of librations in the rotating frame D_c = 3.0 and, from equation 6 of Goldreich *et al.* (*2*), the resonance width $W_c = 2\Delta a_m \lesssim 0.6$ km. This is roughly 25 times smaller than the observed width of the ring arcs. If we assume that the spread in particle semimajor axes is equal to the corotation resonance width, $\Delta a = W_c$, then all particles would have $a > a_{OLR}$, their perturbed orbits would all be in phase, and the spread in their forced eccentricities, Δe_f, due to their differing distances from the Lindblad resonance would yield a ring whose width would vary from W_c at quadrature (where the particle orbits cross) to $W_r = a\Delta e_f$ which can be as large as 12 km. This value is

Table 2. Unofficial nomenclature and longitudinal centers, full lengths at half maximum brightness (FLHM), and center-to-center separations for the five arcs within the N1R ring taken from Fig. 4.

Name	Center (degrees)	FLHM (degrees)	Separation (degrees)	Comments
A1	285.03 ± 0.05	1.0 ± 0.1	—	New leading arc
A2	277.73 ± 0.05	4.1 ± 0.1	7.3 ± 0.1	Former leading arc
A3	265.4 ± 0.5	1.0 ± 0.5	12.4 ± 0.5	Shoulder arc of former middle arc
A4	262.6 ± 0.5	3.0 ± 0.5	2.8 ± 0.7	Main arc of former middle arc
A5	251.88 ± 0.05	9.6 ± 0.1	10.7 ± 0.5	Trailing arc

consistent with the observed width of the arcs (*17*).

Orbit crossing and small-scale arc structure. The arc model described here is unlike other models of moderate-to-high optical depth eccentric rings in which the orbits are confocal and nested with a positive eccentricity gradient. Here, the particle orbits are confocal, exhibit a large negative eccentricity gradient, and cross near quadrature. Germane to this issue and that of corotation resonance shepherding by Galatea are the "clumps" observed within the arcs. These objects are now seen with greater frequency than previously reported. Figure 5 is a cartoon of NA image FDS 11412.46 which captured the trailing arc. Four, but possibly six, clumps appear in the upper part of the image with separations ranging from ~0.5° to 0.8° and a total longitudinal extent of ~3°. This is the group originally reported by Smith *et al.* [see figure 18 in (*3*)]. Another group of two smeared clumps is seen in the lower part of FDS 11412.46. Its longitudinal extent could be ≥2.6°: it is unfortunately truncated by the edge of the frame. The separation between the two clumps in this group is ~1.8°. Yet another smeared clump-like feature has been observed in FDS 11374.45, a 61-s NA image taken of A1 as part of the first retargetted high-resolution series of the arcs. (Figure 4 shows the locations of the two sets of clumps falling within the trailing arc and one clump in the leading arc, all precessed back to epoch under the arcs' mean motion, and indicated by the two hatched regions along the x-axis and a dark solid vertical line at $\lambda = 285.5°$.)

The interpretation was offered that these clumps might be the manifestation of "big" bodies within what is largely a dusty ring—that is, they are dust-sized particles that are concentrated around bigger moonlets—and that these bodies might be the source of dust for the entire ring (*3*). Indeed, perhaps these are source bodies confined to separate corotation zones within the trailing arc. On the other hand, the clumps may in fact be a kinematical effect: the orbits of particles within the arcs are all in phase owing to their interactions with Galatea so that they cross at or near quadrature. The focusing of particles orbits in this manner should lead to ring narrowing and therefore higher-than-average optical depth regions at quadrature (that is, every 4.186°) that travel with the Lindblad pattern speed, not the mean motion of the arcs. (If the latter is the case, then precessing the clumps back to epoch under the arcs' mean motion as was done in Fig. 4 is incorrect.) It is hard to reconcile this hypothesis with the observations that the two groups of clumps seen in A5 consist of several clumps each. Nonetheless, it is noteworthy that the larger of the two groups in A5 is spread around a quadrature point in FDS 11412.46 and the one single clump in A1 falls within 1° of quadrature in FDS 11374.45, observations roughly consistent with orbit focusing.

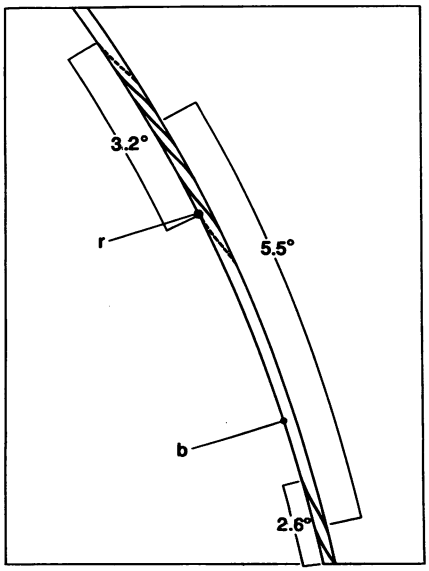

Fig. 5. A cartoon of the entire image FDS 11412.46 taken of A5, the trailing arc, showing the previously reported group of four (possibly six) clumps in the upper portion of the frame (indicated as a hatched region at ~250° in Fig. 4) and another group of two clumps in the lower portion (indicated as a hatched region at ~255° in Fig. 4). The symbol r indicates a camera reseau; the symbol b, a camera blemish.

Outstanding problems and future prospects. Several major difficulties remain with the model proposed here. Collisions among arc particles are likely to occur preferentially near quadrature: that is, twice per orbit. (The low optical depth of the arcs virtually assures that the collision rate would be lower elsewhere in the orbit.) For a relative change in eccentricity across the arcs of roughly $\Delta e/e \sim -0.4$, initial relative velocities in these collisions would be along the radial direction and of magnitude ~2 m s^{-1}. However, finite particle size effects would result in a spread over all dimensions of velocity perturbations to the orbit. As seen from Gauss' equations, even a tangential impulse as small as 0.5 m s^{-1} at quadrature could result in a change in a particle's semimajor axis of 6 km. An alteration in a in excess of W_c would remove the particle from corotation resonance and also from participating in the Lindblad distortion. This is true even if the change in a is less than the width of the Lindblad resonance, W_L. The reasons for this are twofold: (i) If unconfined by the corotation resonance, a particle would drift away from an arc through differential mean motion. For a change in a of 6 km, the timescale to move 4° is approximately a month; (ii) In general, a collision which can alter a significantly would alter the phase and eccentricity of the particle's orbit and act to destroy the Lindblad signature. The time required for a coherent Lindblad signature to grow is tens of synodic periods, each 18 days long. This implies that the particles comprising Neptune's arcs must remain within a region of width W_c ~0.6 km for roughly 1 year in order to participate in the observed Lindblad distortion, obviously inconsistent with the expected timescale of orbital element changes mentioned above.

Another problem exists concerning the lifetime of dust particles in the Neptune arcs. While the collision velocities considered here are not large enough to fracture icy ring particles (*18*), they are probably large enough to create dust. [Indeed, collisions are apparently needed to explain the large dust content of the arcs (*3*).] It is remarkable that these small particles, which in other ring systems have very short lifetimes against perturbations arising from gas drag (as at Uranus), plasma drag (as at Jupiter), and collection onto the surfaces of larger bodies (as at Saturn), are very obviously participating in the Lindblad distortion of Neptune's arcs which, as seen above, takes roughly 1 year to grow. The observation that the trailing arc extends over two or three corotation zones implies that at least some of the particles within this arc find themselves in the unstable zone between potential maxima. These particles are certainly not confined by the CIR and yet they too follow the Lindblad distortion. Either individual dust particles have an arc residence time as long as a year, or they are created with initial orbits very close to those of their parents and at a rate sufficiently high to compensate for what is likely to be rapid removal.

There also remains the question of whether the plane of N1R determined from arc modeling is the ring's Laplace plane or is inclined to this plane. [The Laplace plane of the ring differs from the Neptune equator by ~0.02° almost solely because of the effect of Triton (*9*).] If the former holds, then the identification of the ring pole with its Laplace pole suggests a revision in the Neptune spin pole (Fig. 6). If the latter holds, then the mutual inclination of N1R and Galatea would change with differential nodal precision and

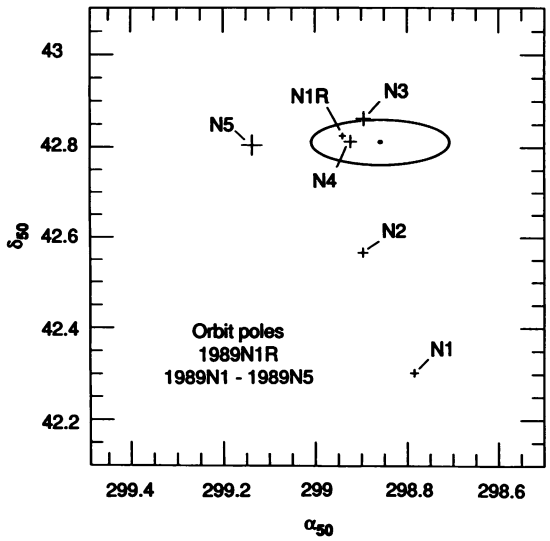

Fig. 6. The distribution of orbit normals for the new Neptunian satellites Proteus (1989N1), Larissa (1989N2), Despoina (1989N3), Galatea (1989N4), and Thalassa (1989N5) (*9*) and the normal to the arc ring, N1R, deduced from this study, at the time of Voyager encounter. The spin pole of Neptune, determined from Voyager 2 trajectory analysis and ground-based observations of Triton (*8*), and its error ellipse are also shown. [The orbit normal for Naiad (1989N6) falls outside the range shown.] If N1R's orbit normal at the time of Voyager encounter were identified as the Laplace pole of the ring [which differs from the Neptune spin pole by only 0.02° (*9*)], then the resulting revision in the Neptune spin pole would reduce the inclinations of satellites Despoina, Galatea, and Thalassa relative to Neptune's equator, indicating that such a revision is likely.

eventually could attain a value as large as ~0.1°. At that time, W_c would increase to ~4 km, causing some arc particles to have $a < a_{OLR}$, erasing the Lindblad signature, changing the appearance of the arcs (*17*) and possibly jeopardizing the model presented here. This issue may be settled with the incorporation into the arc model of Voyager imaging observations made of the narrow ring 1989N2R (*13*) and ground-based arc observations taken 5 years earlier. Over this time, the ring's Laplace pole and Neptune's spin pole would both have precessed around the invariable pole of the Neptune-Triton system in a predictable fashion by ~3°. If N1R is inclined to its Laplace plane, then its pole would precess even more rapidly due simply to the nonspherical gravity field of Neptune. The difference between the two possibilities should be discernible in the combined analysis of Voyager and ground-based observations.

The observation that Neptune's arcs are so few in number and clustered so closely in orbital longitude suggests that they may well have had their origin in the collisional disruption of a small moon, as opposed to the inward drag under either plasma or gas drag forces of small particles initially in orbit around Neptune (*2*). The existence of relatively large satellites within Neptune's Roche zone (*3*), believed to have been dragged there by tidal forces, makes it unlikely that the disruption of a smaller moon would have been tidal or that the disruption and arc formation happened before tidal evolution of the inner Neptunian satellites took place. If the fragments had rather small relative velocities, they might have been readily caught into corotation resonance with Galatea before being able to distribute themselves around the orbit and into a complete ring.

In conclusion, although the arc shepherding model presented here is not without difficulty, it supplies a consistent explanation for the observed 15-km arc radial widths and 30-km radial distortion traveling through the arcs with the angular speed of Galatea, provided that the population of corotation sites by ring material is spatially intermittent and that the spread of particle semimajor axes is ≲0.6 km. Fine-scale structure within the arcs may be the manifestation of the crossing of arc particle orbits or bigger-than-average bodies confined to corotation sites. Finally, the model yields a determination of Galatea's mass density, $\rho_s = 1.0 \pm 0.5$ g cm^{-3}, under the assumption that the mean eccentricity of the arc particles' orbits is determined entirely by the satellite's Lindblad perturbation.

REFERENCES AND NOTES

1. W. B. Hubbard *et al.*, *Nature* **319**, 636 (1986); C. E. Covault *et al.*, *Icarus* **67**, 126 (1986); P. D. Nicholson *et al.*, *Bull. Am. Astron. Soc.* **19**, 888 (1987).
2. P. Goldreich, S. Tremaine, N. Borderies, *Astron. J.* **92**, 490 (1986).
3. B. A. Smith *et al.*, *Science* **246**, 1422 (1989).
4. A. L. Broadfoot *et al.*, *ibid.*, p. 1459; A. L. Lane *et al.*, *ibid.*, p. 1450. These observations indicated an arc core of ~10- to 15-km radial width and normal optical depth τ_N ~0.05, with an apron of tenuous ring material extending ~35 to 50 km exterior to the arc.
5. P. D. Nicholson *et al.*, *Icarus* **87**, 1 (1990). Five years of ground-based data combined with Voyager imaging observations were used to obtain the arcs' mean motion assuming a circular, coplanar orbit. Eccentricities and inclinations less than 0.01 in the orbits of the arcs would not affect these results substantially.
6. A 1981 ground-based arc occultation event [H. J. Reitsema *et al.*, *Science* **215**, 289 (1982)], peculiar in its exceptionally large optical depth and large radial width, was confirmed to be the satellite Larissa (1989N2) imaged by Voyager (*3*).
7. In particular, although it was obvious in Voyager imaging data that Galatea was situated within 900 km of 1989N1R and did have high wave number resonances very close to the ring, the azimuthal scales of these resonances did not seem to match the ~13° "scale" of the arcs (J. J. Lissauer, presentation at the XXVIII Plenary Meeting of the Committee on Space Research, Symposium 4, Neptune after Voyager, The Hague, the Netherlands, July 1990.) Moreover, the satellite did not appear to have a sufficient $M_s i_s^2$ product to produce a ring arc of width W_r ~15 km (*3*). [Another new Neptune satellite, Despoina (1989N3), was found situated interior to 1989N2R by ~700 km, though the currently poor determination of the semimajor axis of 1989N2R prevents a useful search for resonant relations.]
8. R. Jacobson, J. E. Riedel, A. H. Taylor, *Astron. Astrophys.*, in press. Voyager 2 flew closer to Neptune than to any of the other giant planets, and flew within 39,800 km of its largest satellite Triton. This trajectory allowed substantial revisions, and in some cases completely new determinations, of several important Neptune system parameters relevant to orbital dynamics. A combined analysis of the Voyager trajectory and many years worth of ground-based observations of Neptune and Triton have yielded the following values for the Neptune gravitational mass, the second and fourth zonal harmonic coefficients, and the planet's spin pole direction: $GM_p = 6835107 \pm 15$ km^3 s^{-2}; $J_2 = (3410 \pm 9) \times 10^{-6}$ and $J_4 = -(35 \pm 10) \times 10^{-6}$ for a reference radius of $R_p = 25{,}225$ km; and $(\alpha_{50}, \delta_{50}) = (298.66° \pm 0.15°, +42.81° \pm 0.05°)$.
9. W. M. Owen, Jr., R. M. Vaughan, S. P. Synnott, *Astron. J.* **101**, 1511 (1991).
10. P. C. Thomas and J. Veverka, *J. Geophys. Res.*, in press.
11. C. C. Porco and P. Goldreich, *Astron. J.* **93**, 724 (1987).
12. Several notable differences exist between the conventions followed here and those used by P. Goldreich, S. Tremaine, and N. Borderies (*2*). (i) These authors express the resonance conditions and critical arguments for both CIR's and Lindblad resonances in terms of a single m value associated with the CIR alone. (ii) They take m to be an integer that can be either positive or negative, with positive m referring to resonances falling inside the satellite's orbit. (iii) They considered only CIR's associated with a satellite exterior to a set of arcs. In this article, the two resonance types are assigned different resonance wave numbers, m_c and m_L, which are always positive and have the relation $m_c = m_L + 1$. Moreover, the CIR's of a satellite interior to a set of arcs are considered: this is the configuration observed at Neptune. (CER shepherding is impossible with an interior satellite and is not discussed in this article.) In altering the equations of the above authors to match the conventions and arc satellite configuration assumed here, one may take $m = -m_c$ or $m = -(m_L + 1)$ or both.
13. C. C. Porco *et al.*, in preparation.
14. Three parameters were held fixed to obtain this solution: the semimajor axis of the ring, the pattern speed, and the nodal regression rate. The semimajor axis inferred from the arcs' mean motion, $a = 62932.37$ km was used to fix a. (With a allowed to vary, the solution a, 62937.5 ± 5.0 km, is coincident with the inferred value to within the standard error, giving confidence that the inferred value is indeed the correct one.) The pattern speed was held fixed at the mean motion of Galatea: $\Omega_p^L = n_s = 839.6598°$ per day (*9*). The regression rate expected for an inclined orbit at the semimajor axis of N1R owing to Neptune's oblateness is $\dot{\Omega} = -0.676°$ per day. However, if N1R is actually lying within its Laplace plane and its inclination is actually a reflection of a necessary revision in the Neptune spin direction, then the ring would have no natural nodal regression at all. In the expectation that the latter would be the case, the nodal regression rate, $\dot{\Omega}$, was set to zero. (A solution found setting $\dot{\Omega} = -0.676°$ per day was essentially the same as that described in the text with the exception that the nodal line at epoch was found to be $106.5° \pm 1°$.) The inclusion in these solutions of ground-based data, taken as early as 5 years prior to Voyager encounter, will help settle the issue of the regression of the nodes.
15. C. C. Porco, *Adv. Space Res.* **10**, 221 (1990).
16. A reasonable range of satellite density may be obtained from considerations of satellite formation within a CO-rich proto-planetary nebula and, on the other extreme, within a CH_4-rich nebula. The former yields 1.9 g cm^{-3}; the latter yields 1.4 g cm^{-3}.
17. If the ring arc width reflects a spread in semimajor axes of particles comprising the arcs, that is, $W_r = \Delta a$, then it is obvious that some particles would have $a > a_{OLR}$

and some will have $a < a_{OLR}$. Because particles undergoing Lindblad resonant forcing on opposite sides of a resonance would have apsidal lines differing by 180°, a low optical depth ring (in which collisions are infrequent) composed of such particles would exhibit a width that varies over 360°/42° = 8.5714° from essentially zero (at the point where the particle orbits cross) to ~60 km (twice the radial distortion arising from the Lindblad forcing) and back again to zero. As there is an unmistakable and phased 30-km distortion across the arcs, we can dismiss the possibility that $\Delta a = W_r$.

18. D. Davis and E. Ryan, *Icarus* **83**, 156 (1990).

19. V. Haemmerle is acknowledged for extensive help in image data reduction and in the preparation of Fig. 3. I am indebted to P. Goldreich, S. Tremaine, W. Owen, J. Cuzzi, L. Dones, and an anonymous referee for valuable criticisms and suggestions following their readings of a preliminary draft of this article. In particular, I thank W. Owen for many illuminating discussions on his orbit modeling and for kindly providing his results on Neptune satellite orbits prior to publication, and J. Holberg for providing information on the Voyager UVS ring arc occultation. This research was supported by NASA grants no. NAGW-960 and no. NAGW-2342.

22 May 1991; accepted 17 July 1991

Crystal Structure of a CAP-DNA Complex: The DNA Is Bent by 90°

STEVE C. SCHULTZ, GEORGE C. SHIELDS,* THOMAS A. STEITZ

The 3 angstrom resolution crystal structure of the *Escherichia coli* catabolite gene activator protein (CAP) complexed with a 30–base pair DNA sequence shows that the DNA is bent by 90°. This bend results almost entirely from two 40° kinks that occur between TG/CA base pairs at positions 5 and 6 on each side of the dyad axis of the complex. DNA sequence discrimination by CAP derives both from sequence-dependent distortion of the DNA helix and from direct hydrogen-bonding interactions between three protein side chains and the exposed edges of three base pairs in the major groove of the DNA. The structure of this transcription factor–DNA complex provides insights into possible mechanisms of transcription activation.

SEVERE PROTEIN-INDUCED BENDING OF DUPLEX DNA HAS been demonstrated by a variety of biochemical and biophysical techniques (*1–10*), including a low-resolution crystal structure of the nucleosome core particle (*10*). Current high-resolution crystal structures of sequence-specific DNA binding proteins complexed with their DNA binding sites have shown relatively modest departures from straight canonical B-DNA (*11–14*), although the lower resolution (3.9 Å) crystal structure of the λ cro repressor–DNA complex shows an overall bend of ~40° (*15*). We describe a 90° bend in DNA bound specifically to the *E. coli* catabolite gene activator protein (CAP) as observed in a 3 Å resolution crystal structure of this complex.

When CAP [or cAMP (adenosine 3′,5′-monophosphate) receptor protein (CRP)] is complexed with its allosteric effector cAMP, it activates transcription at more than 20 different promoters in *Escherichia coli* [reviewed in (*16, 17*)]. Activation occurs when CAP-cAMP interacts with a specific DNA sequence located at positions that vary from −41 to −103 relative to the transcription start site in various operons.

The crystal structure of CAP-cAMP initially solved at 2.9 Å resolution (*18*) and then refined at 2.6 Å resolution (*19*) showed that the chemically identical 209–amino acid subunits of the CAP dimer consist of a larger amino-terminal domain that binds cAMP and a smaller carboxyl-terminal domain that binds DNA. The CAP-cAMP dimer is structurally asymmetric in these crystals; one subunit has a large cleft between the two domains (the "open" subunit), whereas the other does not (the "closed" subunit). B-DNA was positioned across the helix-turn-helix motifs of CAP according to electrostatic complementarity to generate a model for the CAP-DNA complex (*20, 21*). Subsequent mutagenic experiments are consistent, in part, with specific interactions proposed by this model (*22–27*).

That CAP induces a sharp bend in its DNA binding site has been demonstrated by analyses of the mobility of CAP-DNA complexes in polyacrylamide gels (*4, 5*), electrodicroism measurements of the rotational relaxation times of CAP-DNA complexes (*3*), enhanced rates of cyclization of DNA fragments (*6, 7*), and model building (*21, 28, 29*). Warwicker *et al.* (*28*) constructed CAP-DNA models that bent the DNA by 100° to 160° in order to place the sugar-phosphate backbone in contact with large regions of positive electrostatic potential that exist on the "sides" of CAP. Whereas CAP could only interact with ~20 base pairs of straight DNA, bending the DNA allows for interactions with a 28-bp segment that Liu-Johnson *et al.* (*29*) demonstrated is required for full affinity.

The 3 Å resolution crystal structure of CAP complexed with a 30-bp DNA sequence shows an overall bend of ~90° in the DNA that results primarily from two 40° kinks, one on each side of the dyad axis of the complex. The kinks, which occur in the conserved TGTGA sequence, as well as smaller distortions in other conserved regions of the CAP binding sequence, derive from interactions between the protein and the DNA phosphates and provide, in part, for specific binding through sequence-dependent distortability of the DNA. In addition, sequence specificity is achieved through direct hydrogen-bonding interactions between three side chains emanating from the "recognition" helix of CAP and the exposed edges of three base pairs in the major groove of the DNA helix.

We believe that the bend is an integral part of the mechanism for activation of transcription and propose that in addition to properly orienting CAP for possible interaction with RNA polymerase,

The authors are at Yale University, New Haven, CT 06511. S. C. Schultz and G. C. Shields are in the Department of Molecular Biophysics and Biochemistry and the Howard Hughes Medical Institute and T. A. Steitz is in the Departments of Molecular Biophysics and Biochemistry and of Chemistry and the Howard Hughes Medical Institute.

*Present address: Department of Chemistry, Lake Forest College, Lake Forest, IL 60045.